Environmental Science
Water Research & Technology

Treatment of Brackish-Water Reverse Osmosis Brine Using Only Solar Energy

Journal:	*Environmental Science: Water Research & Technology*
Manuscript ID	EW-ART-04-2021-000291.R2
Article Type:	Paper

SCHOLARONE™
Manuscripts

Ibrahim Abdallah
Associate Director of Wastewater Testbeds
Civil & Environmental Engineering
NSF-NEWT
Rice University
6100 Main St., MS 6398
Houston, TX 77251-1892
P: 573.466-3837
Email: Ibrahim.A.Abdallah@rice.edu

April 26, 2021

The manuscript introduces an experimental work for treating high-salinity brine from reverse osmosis desalination technology at El-Paso, Texas using a nanophotonics solar membrane distillation reactor for the first time. The proposed technology provides low-cot solution using only the solar energy for treating high salinity waters, and is considering a potential solution towards zero/minimum liquid discharge.

Treatment of Brackish-Water Reverse Osmosis Brine Using Only Solar Energy

Ibrahim A. Said[1,2*], Naomi Fuentes[1], Ze He[1,2], Ruikun Xin[1,2], Kuichang Zuo[1,2], W. Shane Walker[1,3], and Qilin Li[1, 2*]

[1]Nanotechnology-Enabled Water Treatment Center (NEWT), Rice University, MS 6398, 6100 Main Street, Houston 77005, United States

[2]Department of Civil and Environmental Engineering, Rice University, MS 519, 6100 Main Street, Houston 77005, United States

[3]Department of Civil Engineering, The University of Texas at El Paso, El Paso, TX 79968-0513, United States

*Corresponding authors: Said (dr.ibrahim.a.said@gmail.com) & Li (qilin.li@rice.edu)

Abstract

Posttreatment of brine produced by reverse osmosis (RO) is a great challenge as it often requires high energy input and works at extreme operating conditions. In this study, brine from a RO plant in El Paso, TX USA was successfully treated using pilot-scale nanophotonics enhanced solar membrane distillation (NESMD) system. The novel NESMD reactor has a nanophotonic membrane surface area of 0.2 m^2 and an internal heat recovery system to recover latent heat released during vapor condensation. By utilizing a sweeping gas operational mode under real solar irradiation (585-827 W/m^2), the NESMD realized successful desalination of RO brine with membrane flux reaching 0.45-0.65 $kg\ m^{-2}\ hr^{-1}$ and total dissolved solids (TDS) removal greater than 99.5% without external heat condenser. The decrease in the feed flow rate to the evaporation channel of the NESMD system led to increasing the gained output ratio (GOR) from 0.35 to 0.62. To the best of our knowledge, this is the largest photothermal reactor utilized for the desalination of real RO brine under practical solar irradiation. Compared with conventional brine treatment processes that require high temperature or pressure, the NESMD desalinates RO brine at a near-ambient temperature and pressure with free solar energy, providing a promising approach for water desalination, and RO brine posttreatment.

Keywords

Solar membrane distillation; pilot-scale; solar irradiation; RO brine; water desalination

1. Introduction

In recent decades, because of the large gap in water demand and supply, water scarcity has been a severe threat to the development of human society. In the latest version of the global risk report by the World Economic Forum, the water crisis is considered one of the top risks in terms of both likelihood of occurring in the next decade and the severity of its impact (1). Unlike other vital commodities such as oil or wheat, water has no alternatives in most situations. Moreover, water is crucial for most productions people are relying on, ranging from food, goods, electricity to manufactured products [2]. According to the analysis of world water demand and supply by the International Water Management Institute (2), not only North Africa and West Asia (NAWA) but also some of the major populated countries, like India and China, are or will be suffering from water deficit. The amount of the affected population is expected to increase continuously. Even in some regions not suffering water scarcity on an annual basis, the affordability of water shows an extreme intra-annual variation due to the seasonal runoff patterns. In a "blue water" scarcity map modeled by Mekonnen (3), two-thirds of people face freshwater scarcity at least one month per year. As a result of water scarcity to such an extent, the cost of drinking waters is exaggerated in some regions. For example, the cost of sufficient municipal drinking water can be 11% to 112% of the typical household income across sub-Saharan Africa (4). An alternative solution for providing drinking water is desalination (5-7). Desalination technologies (including thermal processes such as multi-effect distillation and multistage evaporation and pressure-driven processes such as nanofiltration and reverse osmosis) have been successfully implemented at various scales to purify and desalinate a wide range of source waters (8-10).

Reverse osmosis (RO) consumes 1.5 to 2.5 kWh/m^3 to desalinate seawater; it requires pretreatment to control membrane fouling and scaling. In addition, water recovery of RO desalination systems is between 50 and 85% (depending on feed water quality), and for inland plants, disposal of the brine poses a major challenge and may be very costly.

The State of Texas, USA is a pioneer in utilizing brackish groundwater as a municipal water supply. As of 2006, there were 38 inland brackish water desalination plants in Texas in operation with a total design capacity of 52.3 MGD. These plants dispose of their brines by discharging to surface water, municipal sewer, or evaporation ponds, or in rare situations, the brine can be used for land application (11, 12). Considerations with brine disposal include cost and potential negative impacts on the receiving water body, municipal wastewater treatment plant, or soil quality. The 27.5 MGD Kay Bailey Hutchison brackish groundwater RO plant in El Paso, TX USA started operation in 2007 and the 12 MGD San Antonio Water System (SAWS) brackish groundwater RO plant both use deep-well injection for brine disposal, which incur a large capital cost.

Membrane distillation (MD) is a promising thermal-based membrane technology that realizes the separation of two aqueous solutions by allowing vapor passage of the more volatile component through a hydrophobic microporous membrane under a temperature gradient across the membrane. The hydrophobicity of the membrane allows only the vapor transfer of the volatile liquid, whereby a liquid-vapor interface is formed. Membrane distillation can turn any source of water into clean water such as hypersaline water, oil and gas produced waters, surface water, groundwater, seawater, RO concentrate brines, irrigation drainage water, and other industrial wastewaters. MD works at lower operating temperatures than those of conventional thermal technologies, has a modular configuration and structure that can be easily scaled up or down in treatment capacity, and has relatively low capital costs. Desalinating using a renewable energy source to recover freshwater while minimizing liquid waste disposal at low cost is very attractive for economic, environmental, and regulatory reasons.

We propose a solar-powered treatment technology for the brine stream of reverse osmosis using nanophotonics enhanced solar membrane distillation (NESMD) (13-15). The proposed process efficiently uses sunlight instead of electricity from a power grid or solar photovoltaic panels to drive membrane distillation. It has the benefit of conventional MD processes, i.e., low pressure, low fouling potential, insensitive to total dissolved solids (TDS) concentration, high-recovery, and powered by renewable energy. The susceptibility of the NESMD technology to complex aquatic systems like synthetic hypersaline brine, seawater, and oil-produced water was investigated in previous studies (14, 15). In the case of treating oil-produced waters (total dissolved solids (TDS) of 62,000 – 132,000 ppm) (14), the NESMD showed an excellent rejection both of the Dissolved Organic Carbon and dissolved solids; the hydrophilicity of the NESMD membrane was recovered after washing with de-ionized water. Furthermore, the results showed that the hydrophilic nanophotonics layer appeared to mitigate the wetting of fouling ions into the hydrophobic PTFE layer of the membrane. In a different study (15), NESMD has been employed for treating real seawater from Galveston Bay, Texas, the U.S., and high salinity simulated feedwaters (TDS of 113 200–200 000 ppm) have been tested for long-term testing under the weather conditions of Houston, Texas. The field testing results and observations showed a stable desalination performance of the NESMD reactor in consecutive 5–8 hour operation cycles without operational problems, with a TDS reduction of ≥99.5% in all the field experiments. An average daily membrane flux of ≥0.75 L m^{-2} h^{-1} was achieved at a solar intensity close to 1 kW m^{-2} without an external heat exchanger.

In the light of the previous NESMD studies, the NESMD technology is attracting growing commercial interest due to its special advantages, including 1) superb tolerance to high salinity; 2) off-grid and stand-alone desalination technology; 3) operating at low temperature and atmospheric pressure; 4) no need for external condensers, external heaters, and neither solar collection systems; 5) high quality of the permeate water (TDS removal >99.5%). Hence, the authors extended the applications of the NESMD to treating the discharge brine of reverse osmosis plants.

The current study demonstrates the capability of the NESMD technology for increasing desalination water recovery by treating the RO brine from the brackish water RO plant of Kay Bailey Hutchison Desalination at El Paso, TX USA. The field experiments have been performed outdoor using real solar irradiance at different solar irradiances and feed velocities. This is considered the first time, NESMD was used to treat a discharge real brine from the RO pilot plant. Also, detailed energy balance calculations, for the first time, have been performed to quantify the energy losses from the NESMD reactor to the environment and brine. Those kinds of thermal calculations are considered a great step towards efficient operation of the NESMD with higher water production and lower heat losses. The study is unique in terms of providing a unique solution for the brine management associated with the inland brackish RO water as well as maximizing the water recovery of the RO plants.

2. Materials and Methods

2.1. Nanophotonics Enhanced Solar Membrane Distillation (NESMD) Reactor: Principles and operational mode

NESMD is a novel solar-thermal technology that uses only solar energy for desalination and wastewater treatment(13, 14). It combines both the membrane distillation and solar-thermal collection in a single module using a nanophotonics microporous membrane that serves both as a solar-thermal collector and a desalination membrane. Figure 1A shows the principles of the

NESMD reactor. The photothermal membrane absorbs sunlight across a wide range of the solar spectrum and converts solar energy to thermal energy. This results in an elevated liquid temperature on the feed side of the membrane, and a vapor pressure difference across the membrane, driving vapor transport through the microporous membrane. The condensation of the generated vapor happens on the permeate side of the membrane and generating clean water. The operational mode of the NESMD is similar to the conventional MD, while the key difference is the temperature polarization on the feed side. The temperature polarization is reversed in the case of NESMD as the membrane is the source of heating (13, 16, 17). There are four main configurations of MD or NESMD: sweeping gas membrane distillation (SGMD) (18), vacuum membrane distillation (VMD) (19), air gap membrane distillation (AGMD) (20), direct contact membrane distillation (DCMD) (21, 22). All those different MD configurations are distinguished by modifications implemented on the permeate side of the microporous membrane. Recently, SGMD is gaining a lot of interest due to its lower mass transfer resistance and higher evaporation efficiency (18). In the case of SGMD, an inert gas stream is used to sweep off the vaporized solution out of the permeate chamber and into an external condenser where the purified solution condenses back into a liquid. Hence, in this study, the SGMD using atmospheric air is used in all the NESMD experiments. Implementing SGMD in the current experiments has improved the performance of the NESMD. This could be attributed to the that SGMD has a lower level of conductive-membrane heat loss and lower resistance to mass transfer of the created vapor across the microporous membrane. A higher airflow rate should be avoided to allow the carried vapor by the air to exchange heat with the bottom channel. Also, a lower airflow rate should be avoided to achieve a better mass transfer.

2.2 Preparation and characteristics of the nanophotonics membranes

Hydrophobic microporous membranes were acquired from Pall Corp for developing and fabricating the nanophotonic membranes. This pristine membrane is a composite membrane having a thin polytetrafluoroethylene (PTFE) active layer of 34 µm thickness on top of polypropylene (PP) support sublayer of 184 µm. The porosity and nominal pore size of the membrane are 77% and 0.2 µm, respectively.

The Nanophotonics membranes were developed by a relatively thin (25 µm), optically absorbing, microporous, and a hydrophilic layer of polyvinyl alcohol (PVA) coating deposited onto the PP layer. Functionalized carbon black nanoparticles (Cobalt Corporation) with broadband absorption over the entire solar spectrum were dispersed into the PVA solution(17). Following a pretreatment by polydopamine to ensure adhesion. Figure 2 shows scanning electron microscope (SEM) images of the nanophotonics membrane, where the coating is homogenous over the PP layer. More details about the preparation and characterization of the nanophotonics membranes can be found elsewhere(23, 24). Sunlight is converted into thermal heat on the feed side of the membrane through photothermal heating through the light-absorbing nanomaterials embedded in the PP's porous surface layer. The generated temperature gradient across the photothermal membrane results in water evaporation on the feed side and condensation on the permeate side.

2.3. NESMD Module and Experimental System

NESMD outdoor experiments were conducted using a large-scale plate and frame module with an active membrane surface area of 0.2 m^2. The NESMD module has external dimensions of 1.1 m by 0.38 m with three parallel flow channels (feed/concentrate evaporation, distillate, and feed preheater). Figure 1 (B&C) shows the physical picture of the NESMD module, and Figure 3 shows the process flow diagram of the NESMD process. The three flow channels are (1) evaporation of brackish/saline feed (top) channel between the transmittance window and photothermal membrane; (2) distillate condensation and sweeping air (middle) channel between the membrane and heat exchanger foil; (3) heat exchanger (bottom) channel, where the cold feedwater is preheated with latent heat provided by the condensing vapor in the middle channel. The three-channel design facilitates energy recovery and optimization. During the operation of the NESMD module, the cold feedwater flows first to the third chamber (bottom chamber) to be preheated before entering the top feed chamber. The system has two recirculation loops, the top (hot) recirculation loop to recover the sensible heat from effluent hot concentrate from the evaporation channel, while the bottom recirculation loop is compensating the difference in the flowrates between the top and middle channels. The feed flow rate in the bottom channel is approximately 5 times higher than the feed flow rate in the evaporation channel. The temperature of the feed over the nanophotonics membrane is increasing with increasing the membrane length(13). Thus, since the water flux increases with increasing module length or hydraulic retention time (13), a baffling design is used in the top and bottom channels to achieve adequate channel length while maintaining a reasonable aspect ratio of the module. Both the top and bottom feed-flow channels have been designed and developed with baffles to have a flow cross-section of 1.5 mm height by 21.1 mm width and able to achieve a uniform fluid distribution as well as achieving higher heat and mass transfer coefficients in the bottom channel. The plate and frame three-channel module is developed by using two closing plates of high-density polyethylene with UV resistance from ePlastics (thickness 12.7 mm), three high-temperature silicon rubber sheets (thickness 1.58 mm) for sealing between the flow channels, and a Clear Marine Vinyl film from Marine Vinyl Fabric (thickness 0.5 mm) used as condensing surface. The middle channel is filled with a Nylon net spacer (1.7 mm thickness and 55% porosity) from McMaster-Carr (9318T41), which is necessary for the mechanical supporting of the membrane and condensing foil but also useful for mixing enhancement.

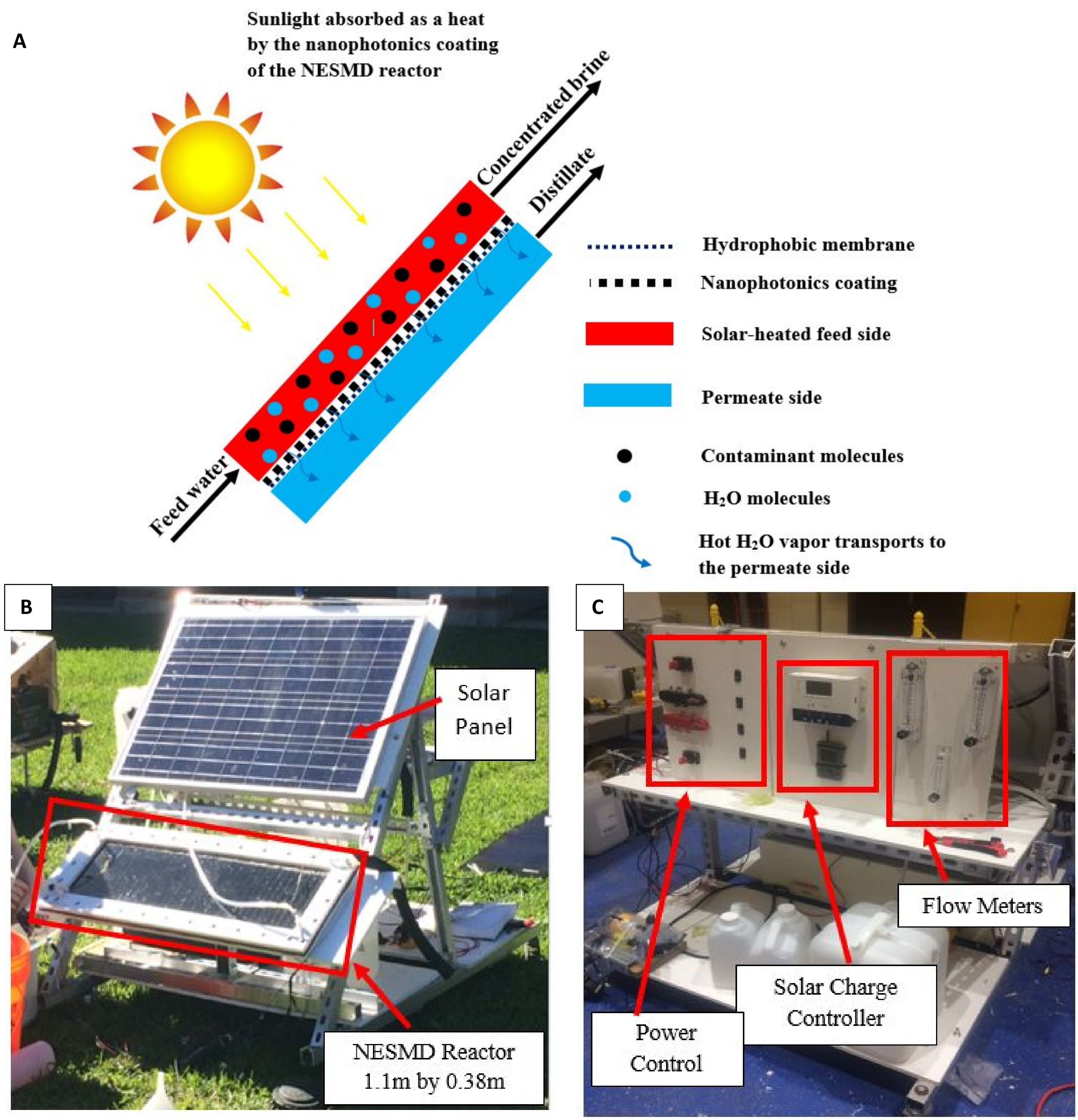

Figure 1. (A). Conceptual illustration of the NESMD reactor. (B) The physical picture of the front view of the NESMD system, including the NESMD reactor and solar panel. (C). The physical picture of the back view of the NESMD reactor, including flow and power control panels.

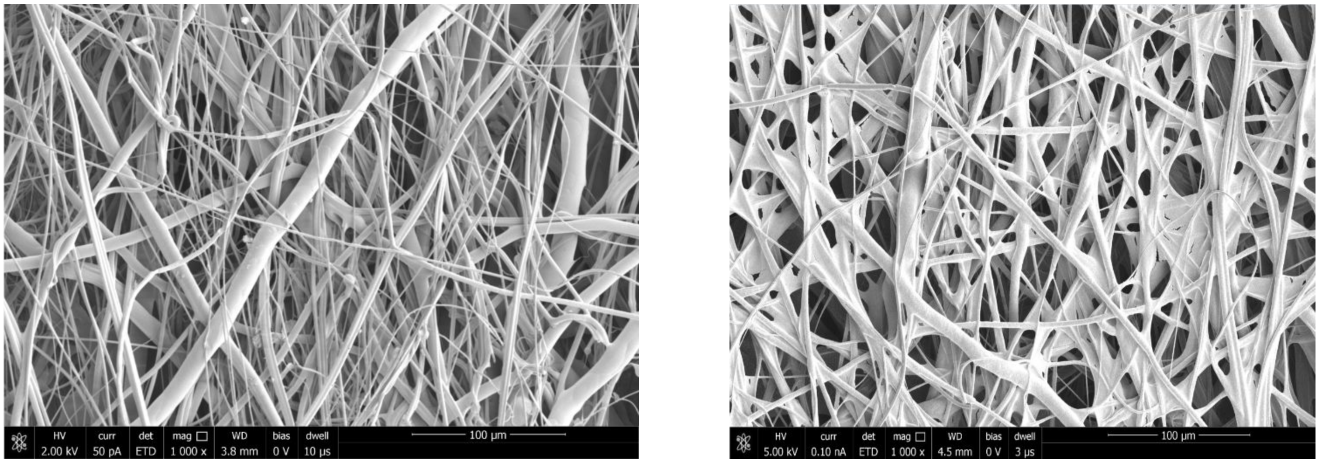

Figure 2. SEM surface images of (left) pristine PP of PTFE membrane, (right) photothermal coating of PP layer (100 μm Resolution)

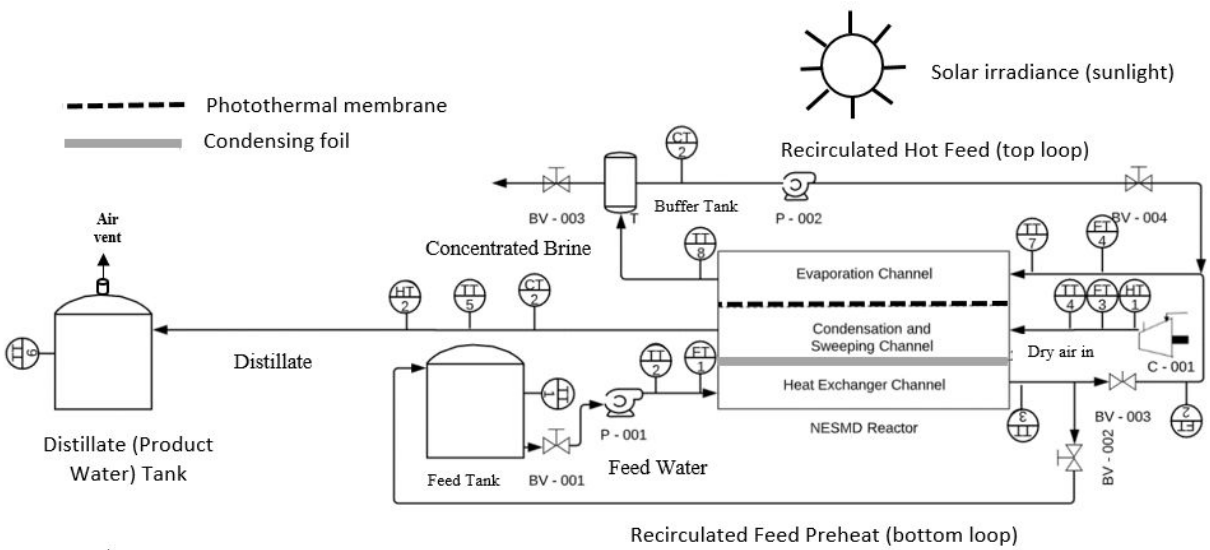

LEGEND	
BV	Ball valve
CT	Conductivity transmitter
FT	Flow transmitter
HT	Humidity transmitter
P - 001	Feedwater pump
P - 002	Recirculating hot feed water pump
TT	Temperature transmitter

Figure 3. Process Flow Diagram of NEMD system

2.4 Process flow control and monitoring

The process flow diagram of the NESMD system (Figure 3) has two recirculation loops as described in section 2.2. Hence, two magnetic-drive pumps (12 Volts, 100W Pan World 30px) are used - one in the bottom (cold feedwater) loop and one in the top (hot feedwater) loop. A 12V DC air compressor (60W RESUN MPQ-904) is used to pump the sweeping air into the middle channel. The measurement system consists of three flow meters for controlling the liquid and airflow rates to the NESMD module, and a series of T-thermocouples (1/16" OD) to track the process temperatures across the three flow channels. All the thermocouples were connected to a data logger with a USB Cable (Onset HOBO UX120-014M). The productivity of the NESMD unit is expressed in terms of water flux, which is defined as the mass of permeate produced per unit membrane area per unit time. Hence, the insulated permeate tank was kept on a weighing balance to monitor the mass of liquid distillate. The increase in the mass of distillate was measured at 15 minutes intervals. Furthermore, the total dissolved solids (TDS) and conductivity for the feed and permeate streams were measured using Cole-Palmer Oakton PC2700 Meter probes in all the experiments.

A solar power irradiance meter (pyranometer) is connected to a data logger to measure solar irradiation. The solar meter has an accuracy of ±10 w/m^2 and is placed in a horizontal plane adjacent to the NESMD reactor. It is worth mentioning that all the environmental parameters, including the ambient temperature, relative humidity, barometric pressure, and ambient wind speed of the air were recorded for every experiment. Table 1 shows the experimental instruments for more details, including the model number, measurement range, application, and accuracy.

Table 1. List of experimental instruments

Instrument	Application	Measurement range	Model number	Accuracy
K-type thermocouple	Temperature	-50 to 700 ^{O}C	TJ36-CASS-116-12	±0.75%
Water liquid flowmeter	Flowrate	0.003 to 0.3 Liter/min	UXcell - s14070200am8595	±3% full scale
Air-gas flowmeter	Flowrate	3 to 30	CNBTR51	±3% full scale

		Liter/min		
Solar power irradiance meter	Solar radiation	400 to 1000 nm	TES132	±5% (±10 w/m^2)
Mass scale	Mass monitoring	0 to 4000 g	CBC8a	±0.1g
Temperature data logger	Temperature	-260 to 1820 ^{O}C	Onset HOBO UX120-014M	0.04 ^{O}C
Humidity meter	Relative humidity (RH)	1% – 99% RH	AcuRite 02067M	±3%RH
Conductivity/TDS meter	TDS and conductivity	Conductivity: 0 - 500 mS/cm TDS: 0.050 ppm (parts per million) to 500 ppt (parts per thousand)	Cole-Palmer Oakton PC2700	Conductivity: ±1% full scale TDS: ±1% full scale
Environmental digital USB data logger	Ambient Temperature	-30 to 70 ^{O}C	TEKCOPLUS	±0.5 ^{O}C
	Ambient relative humidity (RH)	0.1 to 99.9% RH		±3%RH @ 25 ^{O}C and 10-99% RH (others ±5%RH)
	barometric pressure	300 to 1100 hpa		±3.5 hpa @ 0 to 65 ^{O}C and 10 to 90% RH

2.5 Chemical analysis of the RO brine

Two different volume samples of RO brine solutions were used in this study. RO concentrate solutions were obtained from the Kay Bailey Hutchison (KBH) Desalination Plant (El-Paso TX, USA). The RO concentrate solutions were used directly in the NESMD module without any pretreatment. The RO concentrate solutions have a salinity with TDS of 17,440 – 18,550 mg/L with a conductivity ranging between 18.47 – 19.53 mS/cm.

3. Results and discussion

The main aim of this study is to evaluate the technical feasibility of recovering clean and pure water from the real discharge brine of the RO by implementing NESMD technology. Technical simplicity, high quality permeate water output, standing alone over different solar irradiance and environmental parameters are the essential aims which will enable successful application of the NESMD system on a large scale. The heat flux used as heat source of the process will proceed from an nanophotonics coating membrane with the solar irradiance. Hence, it is really important to capture a whole spectrum of the solar irradiance data (sunny, cloudy, and partially cloudy conditions). Field tests under real environmental conditions are very important for assessing the performance of the NESMD with the discharge brine of the RO.

3.1 Desalination performance of NESMD reactor under real solar irradiation

The NESMD experiments have been executed for a typical three days in July of 2019 in the city of Houston, TX, USA (29.7174° N, 95.4018° W). Ambient temperature and solar radiation for a sunny, mostly sunny, and partly cloudy day (07/09/2019, 07/12/2019, and 07/16/2019, respectively) have been reported in the NESMD experiments. The maximum solar irradiance occurred at around 1:00 PM local time. Figure 4 shows the relative humidity of the sweeping air and process temperatures across the three-flow channels of the NESMD reactor. One can remark that the heat exchanger (bottom) channel is getting more latent heat from the generated vapor in the condensation and sweeping (middle) channel, which is very clear in the temperature gained along the bottom channel ($T_{out,bottom}$ and $T_{in,bottom}$). Furthermore, a small difference in the values of the relative humidity of the sweeping air across the middle channel is observed for all experiments. Also, in all the experiments, the relative humidity of sweeping air out is a little bit lower than the relative humidity of the sweeping air inlet. This confirms that the majority of generated vapor in the middle channel is condensed within the middle channel as well as the third channel is working as an excellent heat exchanger. It is really important to monitor the temperature of the process lines across the flow channels, including feed water and sweeping air temperatures. The values of the process temperatures have great indication on the thermal performance of the NESMD reactor. The intensity of the evaporation, condensation, and heat exchange in the top, middle, bottom channels respectively are directly relating to the process temperatures differences. Figures 5-7 show bar graphs for the average process temperatures across the flow channels. It is clear that a small temperature difference is noticed across the top channel for the experiments of 7/12/2019 and 7/16/2019. While the outlet feed temperature is lower than the inlet feed temperature for the experiment of 7/9/2019. These observations could be attributed to the that the heat absorbed by the nanophotonics membrane was used to evaporate the adjacent layer of the liquid at the membrane interface (more evaporation). Also, Figures 5-7 confirm that the outlet temperature from the bottom channel is higher than the inlet for all experiments, while the outlet sweeping air temperature is a little bit higher than the inlet sweeping air. That observations confirm that the middle and bottom channels are working efficiently for condensing the generated vapor and recovering the latent heat (condensation and heat exchange). In all the experiments, the temperature of the permeate stream is equal or lower than the air outlet temperature.

A

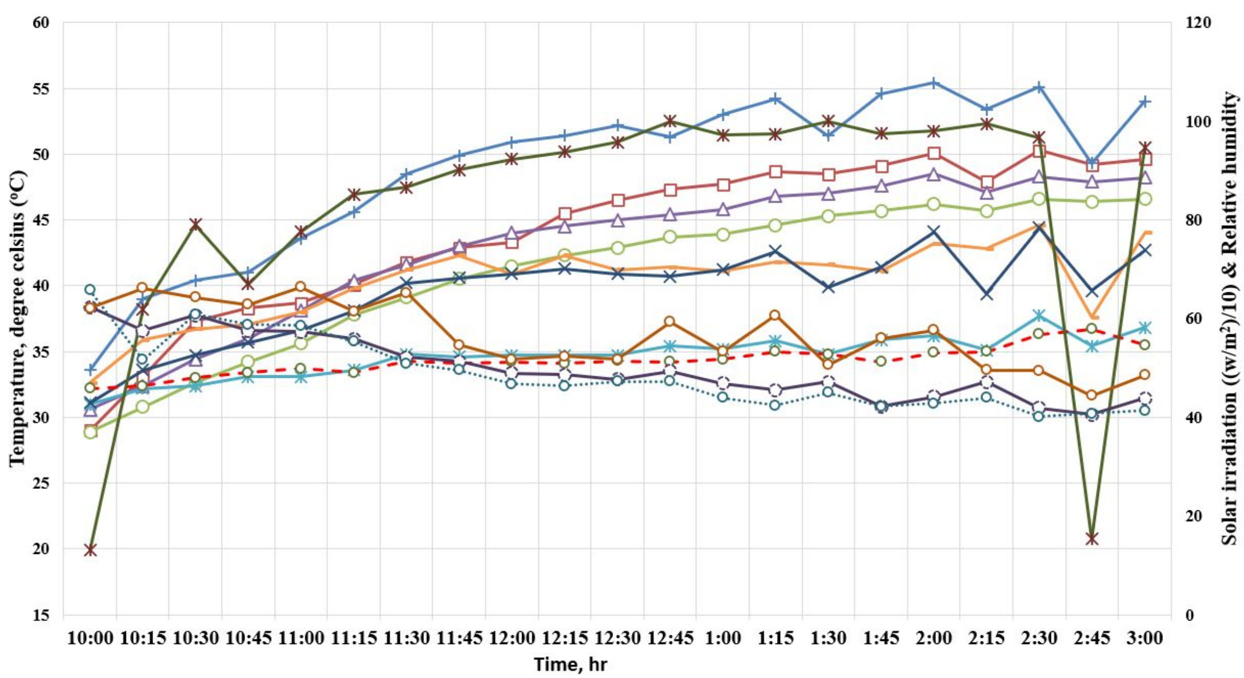

B

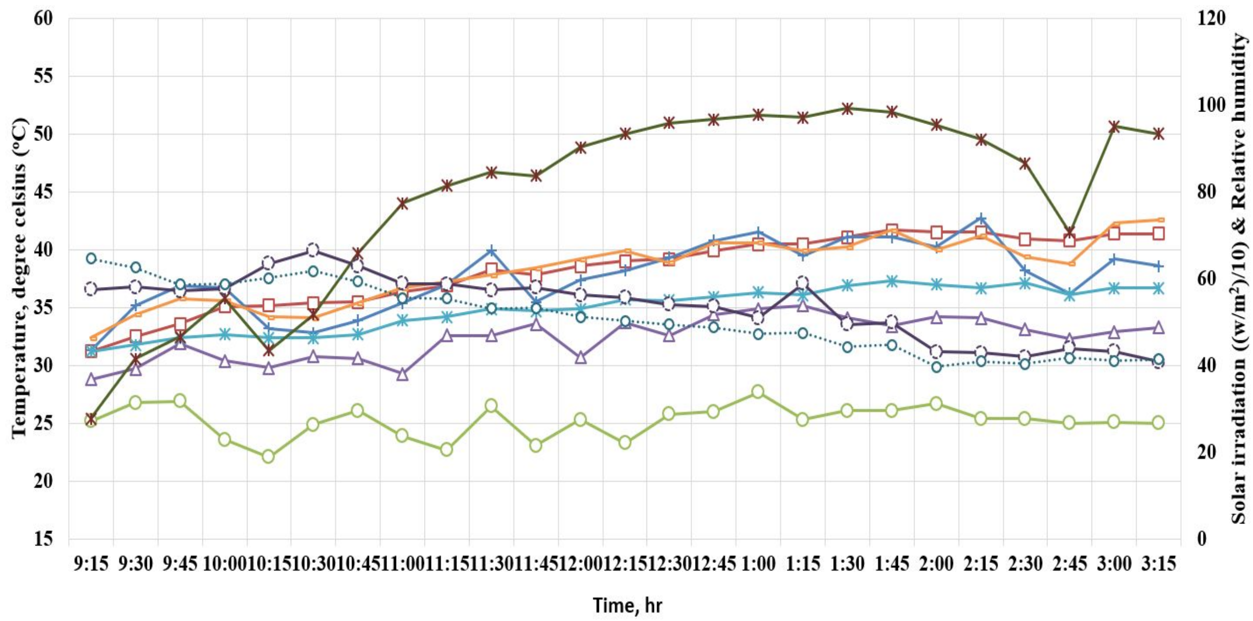
Temperature, degree celsius (ºC)
Solar irradiation ((w/m2)/10) & Relative humidity
Time, hr

C

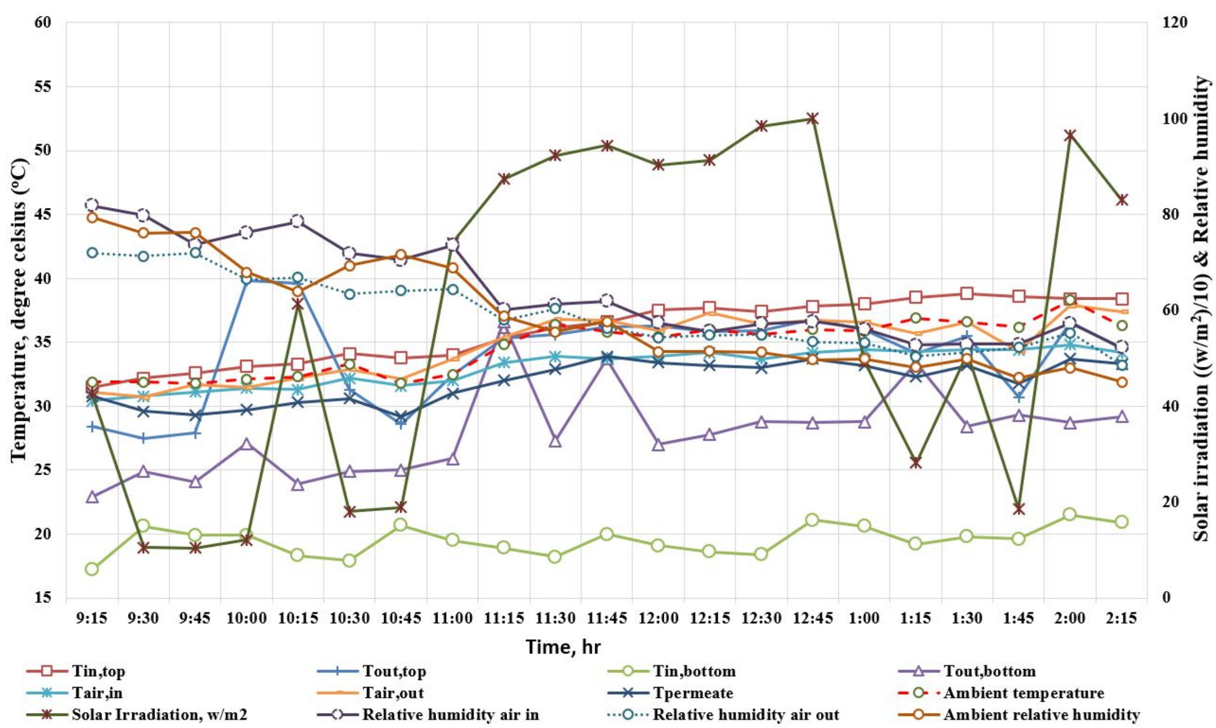
Temperature, degree celsius (ºC)
Solar irradiation ((w/m2)/10) & Relative humidity
Time, hr
Tin,top
Tout,top
Tin,bottom
Tout,bottom
Tair,in
Tair,out
Tpermeate
Ambient temperature
Solar Irradiation, w/m2
Relative humidity air in
Relative humidity air out
Ambient relative humidity

Figure 4. Process field temperature and sweeping gas relative humidity distributions as a function of solar irradiance across the three flow chambers: (A) feed TDS of 17,220 ppm with a TDS removal of 99.5% - flow rates of top channel 3.8 L/hr (cross-flow velocity of 0.03 m/s), bottom channel 17 L/hr (cross-flow velocity of 0.15 m/s), and air 120 L/hr (cross-flow velocity of 0.087 m/s), (7/9/2019); B. feed TDS of 17,440ppm with a TDS removal of 99.5% - flow rates of top channel 1.8 L/hr (cross-flow velocity of 0.016 m/s), bottom channel 17 L/hr (cross-flow velocity of 0.15 m/s), and air 120 L/hr (cross-flow velocity of 0.087 m/s), (7/12/2019); C. feed TDS of 18,550ppm with a TDS removal of 99.6% - flow rates of top channel 1.8 L/hr (cross-flow velocity of 0.016 m/s), bottom channel 17 L/hr (cross-flow velocity of 0.15 m/s), and air 120 L/hr (cross-flow velocity of 0.087 m/s), (7/16/2019).

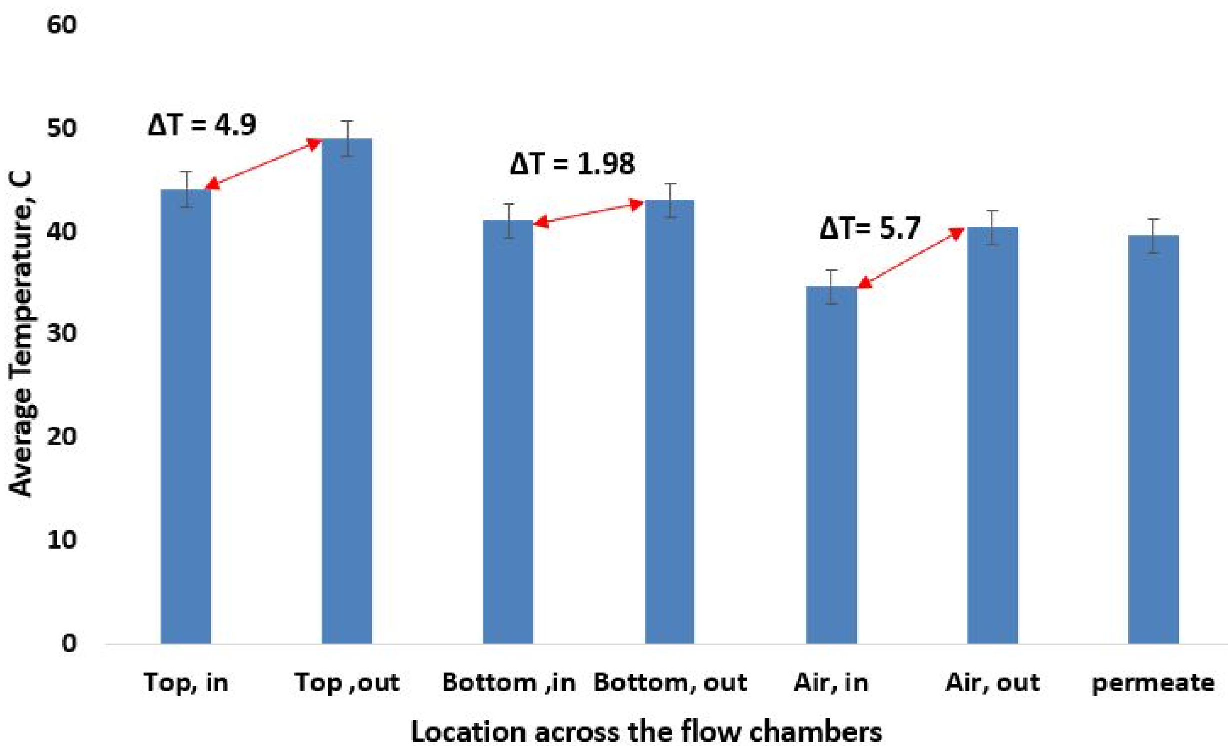

Figure 5. Field temperature of the three flow chambers (TDS of 17,220 ppm with a TDS removal of 99.5% - flow rates of top channel 3.8 L/hr (cross-flow velocity of 0.03 m/s), bottom channel 17 L/hr (cross-flow velocity of 0.016 m/s), and air 120 L/hr(cross-flow velocity of 0.016 m/s)) – 7/9/2019.

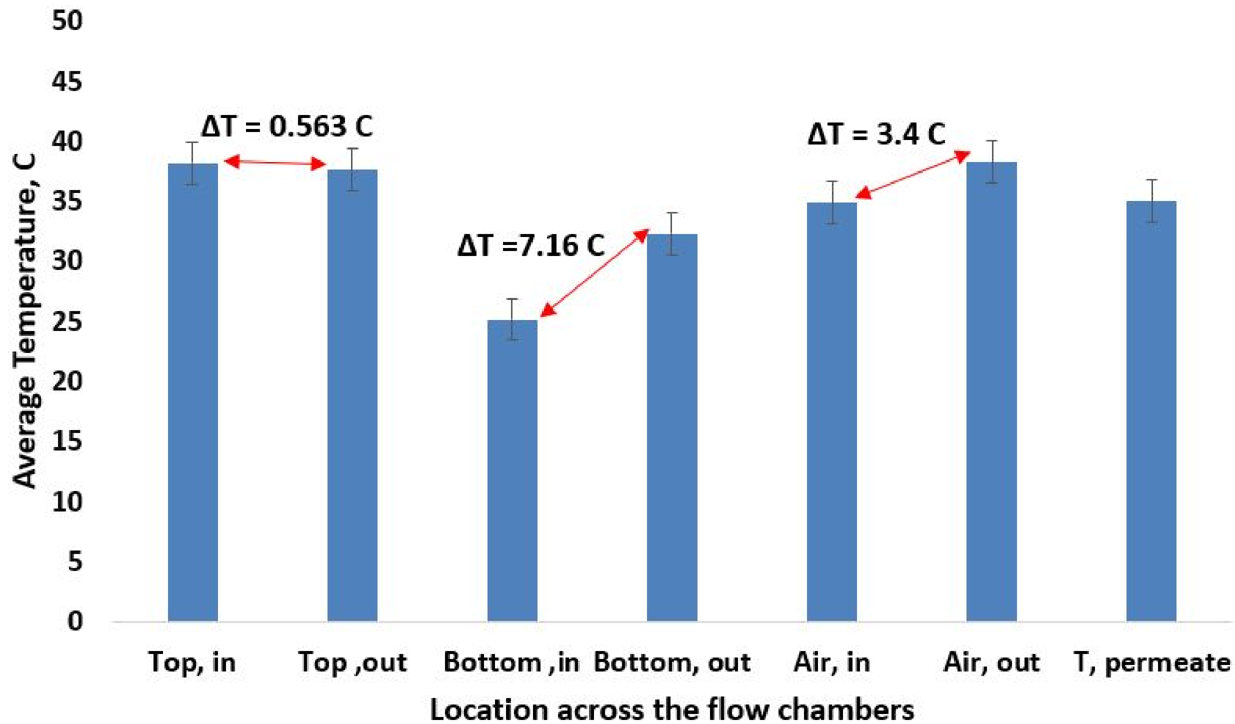

Figure 6. Field temperature of the three flow chambers (TDS of 17,440ppm with a TDS removal of 99.5% - flow rates of top channel 1.8 L/hr (cross-flow velocity of 0.016 m/s), bottom channel 17 L/hr (cross-flow velocity of 0.15 m/s), and air 120 L/hr (cross-flow velocity of 0.087 m/s)) – 7/12/2019.

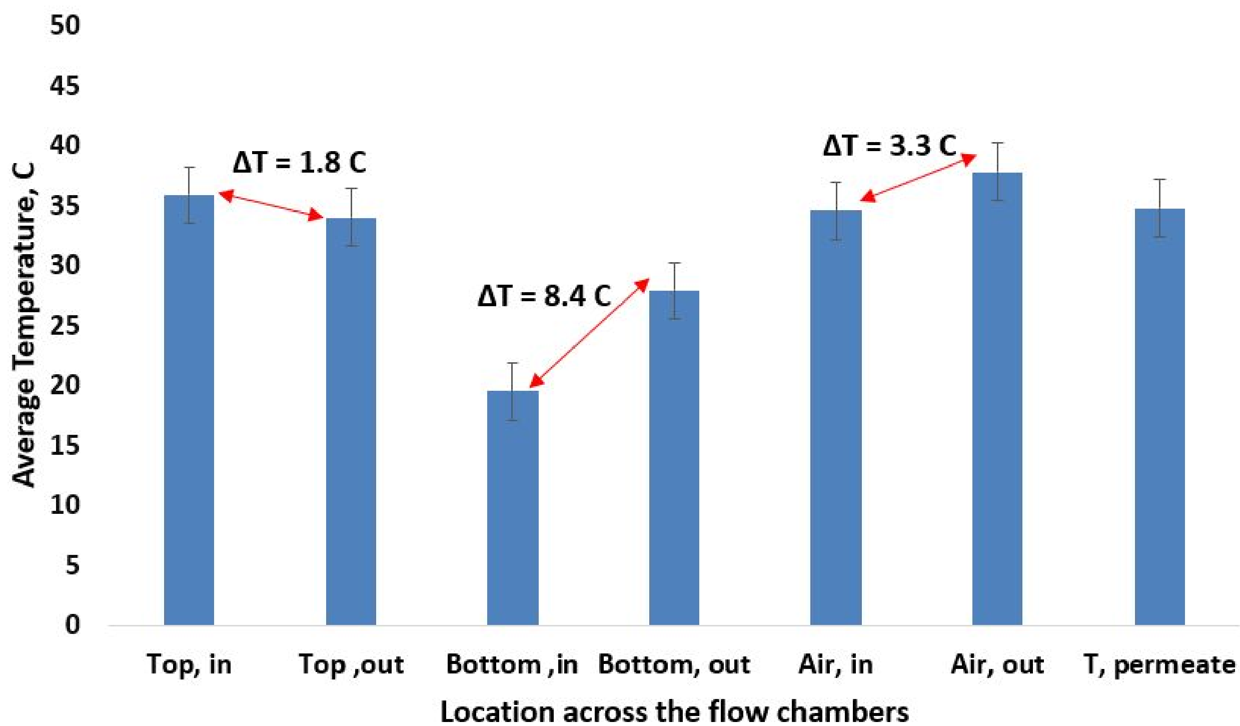

Figure 7. Field temperature of the three flow chambers (TDS of 18,550ppm with a TDS removal of 99.6% - flow rates of top channel 1.8 L/hr (cross-flow velocity of 0.016 m/s) bottom channel 17 L/hr (cross-flow velocity of 0.15 m/s), and air 120 L/hr(cross-flow velocity of 0.087 m/s)) – 7/16/2019.

The production rate of the NESMD in terms of liquid permeate was normalized using the effective membrane surface area (0.2 m^2) and illustrated in Tables 2-3 as a function of the solar irradiation (permeate flux expressed as kg/m^2hr). As shown in Tables 2-3, for a solar irradiance range of 784 -827 w/m^2, the membrane flux was only 0.45 $kg/m^2\ h^1$ at the highest feed flowrate (3.8 L/hr). As the feed flowrate dropped to 1.8 L/hr, the membrane flux increased to 0.65 $kg/m^2\ h^1$. This is attributed to the great increase in the retention time of the feedwater, and consequently higher heat abosprtion and higher vapor pressure at feed side of the top channel which drove the mass transport through the NESMD membrane. It can be also observed that the membrane flux, for the same feed flowrate 1.78 L/hr, increased with the solar irradiance. The reason is that the increased solar irradiance intensifies the feedwater temperature at the feedwater-vapor interface , resulting in higher temperature difference between thetop feed and permeate sides, and consequently higher vapor pressure differences. In another study on a NESMD-SGMD system, An increase in flux had been reported with decreasing the feed flowrate and increasing the solar irradiance (15). Said et al (15) have optimized the cross flow velocity of the air of in the middle channel of NESMD-SGMD (0.087 m/s). Hence, all the field experiments have been performed using a cross-flow velocity of 0.087 m/s, which is corresponding to higher performance stability and higher permeate flux.

In summary, the permeate flux increase with increasing solar irradiance and it also increases with decreasing the feed flow rate to the top channel. The lower the feed flow rate, the higher hydraulic retention time, and consequently higher permeate flux. One more important parameter in membrane distillation technologies is the water recovery ratio (WRR), which indicates the fraction of the feed water that is separated into pure water. The WRR is defined as follows:

$$\text{Water recovery ratio (WRR\%)} = \frac{m_p}{m_f} * 100 \qquad (1)$$

Where m_f is the mass flow rate of the feed water to the top channel, while m_p is the mass flow rate of the distillate. The values of the WRR are also reported in Tables 2-3. It can be seen from Tables 2-3 that the WRR increases with decreasing the feed flow rates to the top channel. The water recovery of the experiment of the feed flow rate of 1.8 L/h (cross-flow velocity of 0.016 m/s) is ~ 3 times the experiments of 3.8 L/hr (cross-flow velocity of 0.03 m/s). This indicates that lower feed flow rates promote more evaporation and consequently higher water recovery. Also, Tables 2-3 summarize all the experiments for different operating conditions, including average solar irradiance, average permeate flux, and TDS removal. Also, all the experiments have a TDS removal of ≥ 95%.

Table 2. A summary of the outdoor lab-scale NESMD experiments (flow rate of the top channel: 3.8 L/hr (cross-flow velocity of 0.03 m/s), *middle channel: 120 L/hr* (cross-flow velocity of 0.087 m/s), *and the bottom channel: 17 L/hr)* (cross-flow velocity of 0.15 m/s)).

Feedwater	TDS Feed, ppm	Average Flux, kg/m²hr	Solar irradiance, w/m²	TDS removal, %	Water recovery ratio, RR%	GOR
Real feed water, KBH, RO concentrate (2L/min air)	17,220 (7/9/2019)	0.45±0.17	827±251	99.5	2.26	0.35

Table 3. A summary of the outdoor lab-scale NESMD experiments (flow rate of the top channel: 1.8 L/h (cross-flow velocity of 0.016 m/s), *middle channel: 120 L/hr* (cross-flow velocity of 0.087 m/s), *and the bottom channel: 17 L/hr* (cross-flow velocity of 0.15 m/s)).

Feedwater	TDS Feed, ppm	Average Flux, kg/m²hr	Solar irradiance, w/m²	TDS removal, %	Water recovery ratio, RR%	GOR
Real feed water, KBH, RO concentrate	17,440 (7/12/2019)	0.65±0.28	784.40±217	99.5	7	0.54
	18,550 (7/16/2019)	0.59±0.16	585±345	99.6	6.30	0.66

It is very clear now that the thermal desalination of the RO brine, using NESMD technology, could be an appropriate feed source for NESMD to further increase the overall water recovery and reduce the marine environmental impacts by reducing the volume of the brine discharge and its process temperature. However, more improvements are required to maximize the water recovery and membrane productivity. One of the key improvement strategies is to recover the latent heat of the vapor using the concept of the multi-effect as well as concentrating the sunlight.

3.2 Energy analysis of the NESMD system

3.2.1. Solar energy and NESMD

The sun is the source of the majority of energy found on earth. The earth receives about 1.74×10^{26} W of the incoming solar irradiance (25). However, 70% is only absorbed by the earth while 30% is reflected. The spectrum of electromagnetic sunlight divides into 5% ultraviolet (UV), 40% visible light, and 55% near-infrared and infrared (NIR and IR). Table 4 summarizes the components of sunlight in terms of wavelength and frequency.

It is worth mentioning that the amount of solar energy received by the NESMD system depends on many parameters, including hour, day, location, season, and an inclination angle as well as weather factors. Some of these factors are shown and discussed in section 3.2 and Figure 4. Cloud is one of the weather factors which has the most significant impact on the solar energy absorbed by the NESMD reactor. The drop in the solar irradiance can reach up to 90% during a thick cloudy condition, while it reaches 10% for a clear day (26). One can remark, in Figure 4, a drop in the readings of solar irradiance in the experiment of July 9th, 2019 at 2:45 PM (CT), and in the experiment of July 16th, 2019 over different time frames of 9:30 AM-10:00 AM (CT), 10:30 AM-10:45 AM (CT), and 1:00 PM–1:45 PM (CT). All that drops in the values of the solar irradiance have a negative impact on the thermal performance of the NESMD system, and consequently the membrane flux. In the next section, a detailed energy balance analysis is performed to quantify the solar energy absorption and losses.

Table 4. Electromagnetic components of the sunlight

Electromagnetic components	% of the total sunlight	Wavelength, nm	Frequency, THz (terahertz)
Ultraviolet (UV)	Less than 5	200-390	790-30,000
Visible light	40	390-780	430-790
Near Infrared (NIR)	55	780-1,400	214-400
Infrared (IR)		1,400-1,000,000	0.3-214

3.2.2 Heat losses calculations

Generally, the heat transfer process in the NESMD system divides into two groups, gained heat transfer and losses heat transfer. The gained heat transfer is responsible for heating the feedwater and generating product water vapor at the liquid-membrane interface. The heat transfer losses include any other forms of heat loss such as heat losses by convection and radiation from the NESMD into the environment as well as heat losses by scattering and reflection. Both the two heat transfer processes are briefly described in this section. Figure 8 illustrates the whole process in the NESMD process in terms of heat losses and heat gained.

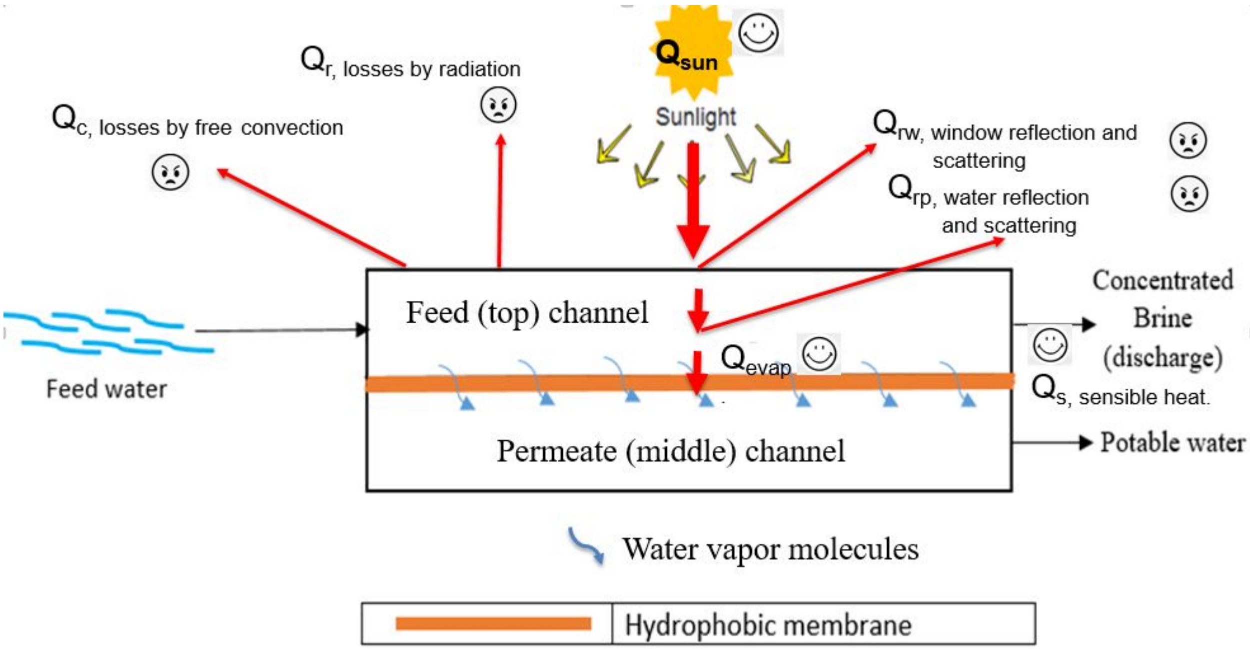

Figure 8. Schematic of energy flux in NESMD reactor (top and middle channels)

The thermal energy losses from the transmittance window of the NESMD reactor to the ambient are represented by free convection and radiation heat transfer modes that are independent of one another. The convective heat transfer losses, Q_c, can be expressed as follows:

$$Q_c = h_c \, A \, (T_s - T_a) \qquad (1)$$

where, T_s and T_a are the surface temperature of the transmittance window and the ambient temperature, respectively, while A is the active membrane surface area. The convective heat transfer coefficient, h_c, is expressed as a function of the relative speed between the transmittance window and the ambient air (υ, m/s) as follows (27):

$$h_c = 3\upsilon + 2.8 \qquad (2)$$

The heat loss by radiation, Q_r, from the outer surface of the Plexiglas transmittance window to the atmosphere is estimated by:

$$Q_c = h_r \, A \, (T_s - T_a) \qquad (3)$$

In the above equation, the radiative heat transfer coefficient, h_r, is calculated by (27):

$$h_r = \sigma\, \xi\, [\frac{(T_s+273)^4 - (T_{sky}+273)^4}{T_s - T_a}] \quad (4)$$

where σ and ξ are the Steven Boltzman constant and emissivity, respectively, while T_{sky} is approximated as follows:

$$T_{sky} = T_a - 6 \quad (5)$$

One more source of the energy losses in the NESMD system is the sunlight scattering and reflection by the water layer of the feedwater on the top of the NESMD membrane. The density of the water is ~800 times denser than the ambient air. As the sunlight enters the water, it interacts with the molecules of the water and salt to cause losses in solar energy. The amount of sunlight reflected depends strongly on the inclination angle of the NESMD reactor, which is 35^0. According to (28, 29) with a reference to the NESMD with an inclination angle of 35^0, 8% of the incident light is scattered and reflected by the water layer (Q_{rw}). Furthermore, there is one more source of energy losses from the NESMD system, which is the sunlight reflected by the transmittance window of the Plexiglas. The light reflected by the Plexiglas sheet depends on the window thickness, angle of incidence, and reflective index. Actual measurement shows that the used transparent Plexiglas sheet with a thickness of up to 6 mm transmits 92% of the incident light striking it at the perpendicular (Q_{rp}) (30).

On the other hand, the rest of solar energy is used to heat the feedwater and consequently generating vapor at the water-membrane interface. The heat of evaporation (Q_e) is calculated as follows:

$$Q_e = J\, A\, \Delta H_v \quad (6)$$

Where J is the membrane flux (kg/m^2 hr), A is the active membrane surface area (m^2), and ΔH_v is the latent heat of vaporization (kJ/kg). Furthermore, the sensible heat gained by the feedwater (Q_s) depends on the temperature difference of the feed across the top channel, heat capacity of the feedwater (C_p), and mass flow rate of the feed ($\dot{m}$). The Q_s is calculated by:

$$Q_s = \dot{m}\, C_p\, (T_{F,effluent} - T_{F,\,influent}) \quad (7)$$

Thermal losses efficiency, η, of the NESMD reactor is one of the key parameters used to assess the performance of the solar thermal desalination process. The η can be calculated as follows:

$$\eta = [\frac{Q_c + Q_r + Q_{rw} + Q_{rp}}{I\, A}]*100 \quad (8)$$

The results showed that heat losses compose up to 64% of the overall solar heat amount. In other solarthermal desalination technologies such as solar stills, the heat losses compose 70-80% towards overall solar heat input (26).

3.2.3 Gained-Output Ratio of the NESMD

The energy efficiency of the NESMD system was evaluated using gained output ratio (GOR) which is the most important performance parameter in thermal desalination technologies to gauge the energy efficiency of MD. GOR is defined as the latent heat required to evaporate all the mass flow rate of clean water produced compared with the external energy added to the NESMD system. A higher GOR can be attained by recovering the latent heat from the permeate vapor to preheating the feed solution. The GOR is defined as follows:

$$GOR = \frac{\Delta H_v \cdot \dot{m}_v}{Q_{solar}\ A_m} \qquad (2)$$

where ΔH_v (kJ/kg) is the latent heat of vaporization of water, $\dot{m}_v$ (kg/s) is the mass flow rate of clean water produced by the NESMD system, Q_{solar} (W/m^2) is ambient solar radiation, and A_m (m^2) is the surface area of the NESMD membrane. Tables 2-3 list the values of the GOR for all the experiments. As shown in Tables 3-4, decreasing the feed flow rates from 3.8 L/h (cross-flow velocity of 0.03 m/s) to 1.8 L/h (cross-flow velocity of 0.016 m/s) resulted in increasing the GOR from 0.32 (experiment of 7/9/2020) to 0.54 (7/12/2020) and 0.66 (7/16/2020). The lower feed flow rate to the top channel resulted in higher residence time that led to more sunlight absorption, and consequently higher vapor flux.

Conclusions

A nanophotonics enhanced solar membrane distillation (NESMD) reactor having a total effective membrane surface area of 0.2 m^2 with an internal heat recovery system has been designed, developed, and tested without an external heater or external condenser. Hence, the solar collection, membrane distillation, heat recovery, and condensation all happened inside the NESMD reactor. A complete design, process flow diagram, electrical diagram, and material selection have been outlined. In this study, natural reverse osmosis brine from the brackish desalination plant at El Paso TX, USA (TDS 17,220 – 18,550 mg/L) has been desalinated by using the NESMD reactor. The current research validates the applicability of NESMD to desalinate natural RO brine and maximize the water recovery from the RO systems using only solar energy. The preliminary field data released the following findings:

- The NESMD reactor continuously operated for five to six hours outdoor each of three days with no operational problems. This is a good indication of the durability and mechanical integrity of the NESMD system as well as the photothermal coating stability.
- The NESMD was able to produce clean and pure water (conductivity, lower than 15 µS cm− 1) from the high concentrate brackish RO discharge brine (conductivity, 18.47-19.53 mS cm^{-1})
- The average feed TDS was approximately 18 g/L with an average TDS removal of 99.5%, producing product water with an average TDS of70 mg/L, meeting the World Health Organization (WHO) drinking water standard.
- Steady-state average membrane flux of 0.46-0.65 kg m^{-2} hr^{-1} was observed at a solar intensity of 585-827 W/m^2 without an external condenser.
- Lowering the feed flow rate to the evaporation channel has a positive effect on increasing the GOR;
- The energy balance analysis showed that heat losses compose up to 64% of the overall solar heat amount, and that would be required extensive strategic energy management.
- The technology is still in an early stage and more improvements are required to improve productivity. One of the key improvement strategies is to recover the latent heat of the vapor using the concept of the multi-effect as well as concentrating the sunlight.

Acknowledgment

This work was funded by the U.S. Department of Energy – Solar Energy Technologies Office (Award # DE-EE0008397) and NSF NERC on Nanotechnology-Enabled Water Treatment (NEWT-EEC 1449500).

Conflict of Interest

The authors declare no conflict of interest

References

1. Forum WE. Global Risks Report 2020.
2. David Seckler, Amarasinghe U, David Molden, Silva Rd, Barker R. World Water Demand and Supply, 1990 to 2025: Scenarios and Issues. International Water Management Institute. 1988.

3. Mekonnen MM, Hoekstra AY. Four billion people facing severe water scarcity. Science Advances. 2016;2(2):1-6.
4. Mitlin D, Walnycki A. Why is water still unaffordable for sub-Saharan Africa's urban poor? IIED Briefing. 2016:1-4.
5. Ghalavand Y, Hatamipour MS, Rahimi A. A review on energy consumption of desalination processes, Desalination and Water Treatment. 2015;54:1526-41.
6. Alkaisi A, Mossad R, A. Sharifian-Barforoush. A Review of the Water Desalination Systems. Integrated with Renewable Energy, Energy Procedia. 2017;110:268-74.
7. Association ID. International Desalination Association and Global Water Intelligence Release New Data in 30th Worldwide Desalting Inventory. 2017.
8. Malaeb L, Ayoub GM. Reverse osmosis technology for water treatment: State of the art review. Desalination. Desalination. 2011;267(1):1-8.
9. Global Water Desalination Market and Its Related Technologies (Reverse Osmosis, Multi-stage Flash Distillation, Multi Effect Distillation, Hybrid, Electrodialysis), Its Source (Seawater, Brackish Water), Regional Trends and Forecast 2018 to 2025. Adroit Market research. 2020;https://www.adroitmarketresearch.com/industry-reports/water-desalination-market.
10. Raluy G, Serra L, Uche J. Life cycle assessment of MSF, MED and RO desalination technologies. Energy. 2006;31(13):2361-72.
11. Bruggen BVd, Vandecasteele C. Distillation vs. membrane filtration: overview of process evolutions in seawater desalination. Desalination. 2002;143(3):207-18.
12. Kim YM, Kim SJ, Kim YS, Lee S, Kim IS, Kim JH. Overview of systems engineering approaches for large scale seawater desalination plant with reverse osmosis network. Desalination. 2009;238:312-32.
13. Said IA, Wang S, Li Q. Field Demonstration of a Nanophotonics-Enabled Solar Membrane Distillation Reactor for Desalination. Ind Eng Chem Res. 2019;58(40):18829-35.
14. A.Said I, R.Chomiak T, He Z, Li Q. Low-Cost High-Efficiency Solar Membrane Distillation For Treatment of Oil Produced Waters. Separation and Purification Technology. 2020;250(117170).
15. Said IA, Fuentes N, He Z, Xin R, Zuo K, Li Q. Low-cost desalination of seawater and hypersaline brine using nanophotonics enhanced solar energy membrane distillation. Environmental Science: Water Research & Technology. 2020;6(8):2180-96.
16. Wu J, Zodrow KR, Szemraj PB, Li aQ. Photothermal nanocomposite membranes for direct solar membrane distillation. Journal of Materials Chemistry A. 2017;5(45):23712-9.
17. Dongare PD, Alabastri A, Pedersen S, Zodrow KR, Hogan NJ, Neumann O, et al. Nanophotonics-enabled solar membrane distillation for off-grid water purification. Proceedings of the National Academy of Sciences of the United States of America. 2017;114:6936-41.
18. Said IA, Chomiak T, Floyd J, Li Q. Sweeping Gas Membrane Distillation (SGMD) for Wastewater Treatment, Concentration, and Desalination: A Comprehensive Review. Chemical Engineering & Processing: Process Intensification. 2020;153(107960):https://doi.org/10.1016/j.cep.2020.107960.
19. Chiam C-K, Sarbatly R. Vacuum membrane distillation processes for aqueous solution treatment—A review. Chemical Engineering and Processing: Process Intensification. 2013;74:27-54.
20. Shahua VT, Thombre SB. Air gap membrane distillation: A review. Journal of Renewable and Sustainable Energy. 2019;11(4):045901.
21. Alkhudhiri A, Darwish N, Hilal N. Membrane distillation: A comprehensive review. Desalination. 2012;287:2–18.
22. Lagana F, Barbieri G, E. Drioli. Direct contact membrane distillation: modelling and concentration experiments. J Membr Sci 2000;166:1-11.
23. Kellogg B. Development and Evaluation of Electrospun Nanocomposite Coatings for Solar Membrane Distillation. Rice University: Rice University; 2018.

24. Wu, K. R. Zodrow, Szemraj PB, Li Q. Photothermal nanocomposite membranes for direct solar membrane distillation. Journal of Materials Chemistry A. 2017;5:23712-9.
25. Smil V. General Energetics Energy in the Biosphere and Civilization. John Wiley, New York. 1991.
26. Arsen H, Hakobyan A. New portable seawater desalination solar plant based on membrane distillation technology. CreateSpace Independent Publishing Platform, ISBN-13: 978-1467950374 2011.
27. Sharshir SW, Elsheikhd AH, Peng G, Yang N, El-Samadony MOA, Kabeel AE. Thermal performance and exergy analysis of solar stills – A review. Renewable and Sustainable Energy Reviews 2017;73:521–44.
28. Anthoni JF. Water and light. http://wwwseafriendsorgnz/phgraph/waterhtm. 2005.
29. Encyclopædia Britannica, Inc. 2010;XXXI(15TH):1-32,640.
30. Arkema. Plexiglas Acrylic Sheet: Optical & Transmission Characteristics. Philadelphia, PA; 2000.